What controls the Fe II strength in active galactic nuclei?

Xiaobo Dong[1,4], Jianguo Wang[2,1,7], Tinggui Wang[1,4], Huiyuan Wang[1,4], Xiaohui Fan[3,5], Hongyan Zhou[1,4,6], and Weimin Yuan[2]

xbdong@ustc.edu.cn

ABSTRACT

We have investigated the correlations of the equivalent widths (EWs) of narrow and broad Fe II emission lines and the Fe II/Mg II intensity ratio with fundamental physical parameters of active galactic nuclei (AGNs), luminosity (L), black hole mass ($M_{\rm BH}$) and Eddington ratio ($L/L_{\rm Edd}$), using a homogenous sample of $z \leq 0.8$ Seyfert 1 galaxies and QSOs in the spectroscopic data set of Sloan Digital Sky Survey Fourth Data Release (SDSS DR4). The sample comprises 4178 spectra that are selected to suffer little from the host-galaxy starlight contamination. We find that the strongest correlations of almost all the emission-line intensity ratios and EWs are with $L/L_{\rm Edd}$, either positively (e.g. Fe II EW) or negatively (e.g. Mg II EW), rather than with L or $M_{\rm BH}$; In particular, the intensity ratios of both the ultraviolet and optical Fe II emissions to Mg II λ2800 correlate quite tightly with $L/L_{\rm Edd}$ (e.g., Spearman $r_{\rm s}$ = 0.74 for the [narrow Fe II]/Mg II – $L/L_{\rm Edd}$ correlation). We have also investigated the Fe II emission in the full sample of about 27,000 type 2 AGNs in the SDSS DR4, and find that no Fe II is detected at 3σ significance. We argue that (1) the narrow-line Fe II in AGNs originates purely from the inner narrow-line region on scales less than the torus whereas the sites of the broad-line Fe II are likely not unique; (2) The variation of the emission-line strength in AGNs are regulated by $L/L_{\rm Edd}$ because it governs the global distributions of the properties (particularly column density) of the clouds gravitationally bound in

[1]Center for Astrophysics, University of Science and Technology of China, Hefei, Anhui 230026, China

[2]National Astronomical Observatories/Yunnan Observatory, Chinese Academy of Sciences, P.O. Box 110, Kunming, Yunnan 650011, China

[3]Steward Observatory, The University of Arizona, Tucson, AZ 85721, USA

[4]Key Laboratory for Research in Galaxies and Cosmology, The University of Sciences and Technology of China, Chinese Academy of Sciences, Hefei, Anhui 230026, China

[5]Max Planck Institute for Astronomy, D-69120, Heidelberg, Germany

[6]Max-Planck-Institut für extraterrestrische Physik, Giessenbachstrasse 1, 85748 Garching, Germany

[7]Graduate School of the Chinese Academy of Sciences, 19A Yuquan Road, P.O.Box 3908, Beijing 100039, China

the line-emitting region; (3) The systematic dependence on $L/L_{\rm Edd}$ must be corrected for when using the Fe II/Mg II intensity ratio as a measure of the Fe/Mg abundance ratio to study the history of chemical evolution of quasar environment.

Subject headings: radiation, accretion – galaxies: active – quasars: emission lines – quasars: general

1. Introduction

Fe II multiplet emission is a prominent feature in the ultraviolet (UV) to optical spectra of most active galactic nuclei (AGNs), including QSOs at redshifts as high as $\gtrsim 6$ (e.g., Freudling et al. 2003, Barth et al. 2003, Iwamuro et al. 2004, Jiang et al. 2007, Kurk et al. 2007). Its equivalent width (EW) varies significantly from object to object (e.g., from > 100 Å to undetectable for the emission in the 4434–4684Å region [hereafter λ4570]; Boroson & Green 1992, hereafter BG92). Fe II is an important probe of AGN physics. For example, BG92 showed that the relative strength of the Fe II λ4570 emission is a dominating variable in the first principal component (PC1) in their analysis of the correlation matrix of QSO properties which is generally believed to be linked to certain fundamental parameter of accretion process (e.g., the relative accretion rate, often expressed as $L/L_{\rm Edd}$ or L/M; Sulentic et al. 2000, Boroson 2002). More importantly, Fe II emission relative to that of α-elements (e.g. Mg II) can be considered to be an observational proxy of the Fe/α abundance ratio. If iron is mainly produced by Type 1a supernovae that have long-lived progenitors, this ratio would have a characteristic delay of ~ 1 Gyr from the initial starburst in the quasar host environment, based on chemical evolution models. Thus Fe II emission in principle can serve as a cosmic clock to constrain the age of QSOs and the epoch of the first star formation of their host galaxies (Hamann & Ferland 1993; and cf., e.g., Matteucci & Recchi 2001).

However, the ionization and excitation mechanisms of the Fe II emission are very complex due to the low ionization potential of Fe^0 atom (7.9 eV), the low energy levels of various excited sates of Fe^+ ion, and particularly the complexity of its atomic structure (see Baldwin et al. 2004, Collin & Joly 2000 and references therein, Joly et al. 2008). Thus the conversion from Fe II emission to iron abundance is not straightforward (e.g. Verner et al. 2004, Baldwin et al. 2004). Furthermore, it is possible that Fe II emission of AGNs arises from a number of different sites with similarly suitable excitation conditions, including gaseous clouds gravitationally bound in the narrow-line and broad-line region (NLR and BLR), (the base of) outflows, and the surface of the accretion disk (AD) [see, e.g., Collin-Souffrin 1987 et seq., Murray & Chiang 1997, Matsuoka et al. 2007, Zhang et al. 2007]. This has already been hinted by the reverberation observations of Fe II emission, particularly of its optical component, since the cross-correlation function appears to be flat-topped (Vestergarrd & Peterson 2005, Kuehn et al. 2008; see also Kollatschny & Welsh 2001, Wang et

al. 2005). Therefore, to use of Fe II emission as a proxy of Fe abundance and further as a cosmic clock requires a better understanding of its emission mechanism. In fact, it is well known that the Fe II/Mg II ratios of QSOs at the same redshift have a rather large scatter (e.g. Iwamuro et al. 2004, Leighly & Moore 2006).

It is also possible that the excitation mechanisms and sites of Fe II emission are well governed by certain fundamental parameters (such as Eddington ratio)[1] due to certain self-regulation mechanisms that maintain the normal dynamically quasi-steady (or even quasi-virialized) states of the gas surrounding the central engine of AGNs. It is well-known for decades that QSO spectra are remarkably similar, at the zeroth-order approximation, with emission lines of similar intensity ratios sitting atop a blue continuum regardless of their luminosities and redshifts (Davidson & Netzer 1979, Korista 1999, Dong et al. 2008; see more evidence and insightful arguments for the similarity in Gaskell et al. 2004, Gaskell et al. 2007, Gaskell & Benker 2008).[2] This similarity means that the integrated spectra and global properties of QSOs are rather insensitive to the detailed distributions of various gas properties and the 'microscopic' physical processes taking placing in the line-emitting region of AGNs; instead, they are governed by the powerful selection mechanisms introduced by the atomic physics (albeit not exactly identified yet), as proposed by Baldwin et al. (1995) in the "locally optimally-emitting clouds" model that has reproduced the overall QSO broad-line spectra (e.g. Korista & Goad 2000). If the variations of the emission lines, particularly, the narrow-line or broad-line Fe II emissions, are in a similar situation — i.e., their variations are indeed governed by certain self-regulation mechanisms and thus are regular, we may calibrate the translation from Fe II emission to abundance and constrain chemical evolution in the quasar environment.

Motivated by these considerations, we carry out a systematic study on the strengths of UV

---

[1] Eddington ratio ($\ell \equiv L/L_{\rm Edd}$) is the ratio between the bolometric and Eddington luminosities. Eddington luminosity ($L_{\rm Edd}$), by definition, is the luminosity at which the gravity of the central source acting on an electron–proton pair (i.e. fully ionized gas) is balanced by the radiation pressure due to electron Thomson scattering; $L_{\rm Edd} = 4\pi GcMm_{\rm p}/\sigma_{\rm T}$, where G, c, M, $m_{\rm p}$, $\sigma_{\rm T}$ are the gravitational constant, speed of light, mass of the central source, proton mass, Thomson scattering cross-section, respectively. In accretion-powered radiation systems, $L/L_{\rm Edd}$ is often referred to as *dimensionless accretion rate* $\dot{m}$ (the relative accretion rate normalized by Eddington accretion rate $\dot{M}_{\rm Edd}$, $\dot{m} \equiv \dot{M}/\dot{M}_{Edd} = \eta c^2 \dot{M}/L_{\rm Edd}$, $\dot{M}$ being mass accretion rate and η the accretion efficiency) as $\dot{m}$ is not an observable; yet the two notations are different both in meaning and in scope of application. Even in the accretion-powered radiation systems like AGNs, $L/L_{\rm Edd}$ (L) is not equivalent to $\dot{m}$ ($\dot{M}$) except in the simple thin accretion disk model of Shakura & Sunyaev (1973). Therefore, we call $L/L_{\rm Edd}$ *dimensionless luminosity* (ℓ). For clarification or for the ease of notation, below we use $L/L_{\rm Edd}$ and ℓ alternately.

[2] The zeroth-order similarity perhaps holds even for low-luminosity and low-accretion AGNs (see, e.g., Moran et al. 1999 for NGC 4395, Maoz 2007). If it is the case, it means that the global spectral energy distribution and emission lines of AGNs is quite insensitive to $M_{\rm BH}$ in the range of $10^5 - 10^{10}\ M_\odot$ and $L/L_{\rm Edd}$ in the range of $0.001 - 1$.

and optical Fe II emissions, by taking advantage of the unprecedented spectroscopic data from the Sloan Digital Sky Survey (York et al. 2000). Particularly, using the analysis of Véron-Cetty et al. (2004), we are able to study narrow-line Fe II emission systematically for the first time. The paper is organized as follows: In section 2 we describe the selection criteria of the sample, the spectral processing, and correlation and regression analyses. Section 3 presents the results and our discussions. Section 4 is our brief conclusions and implications. Throughout this paper, we use a cosmology with H_0=70 km s^{-1} Mpc^{-1}, $\Omega_{\rm M}$=0.3 and Ω_Λ=0.7.

2. Data analysis

2.1. Sample and measurements

2.1.1. Sample construction

We first construct a homogenous sample of Seyfert 1s and QSOs (namely type-1 AGNs) from the spectral data set of the SDSS Fourth Data Release (Adelman-McCarthy et al. 2006), according to the following criteria: (1) redshift $z \leq 0.8$; (2) the median signal-to-noise ratio (S/N) ≥ 10 per pixel in the optical Fe II and Hβ region (4400–5400Å); (3) the rest-frame absorption-line equivalent widths (EWs) of Ca K (3934Å), Ca K + Hϵ (3970Å) and Hδ (4102Å) $< 2\sigma$. The redshift cut is set to ensure the Hβ and Fe II λ4570 multiplets are present in the SDSS spectra; the S/N criterion allows proper placement of local continua and the accurate measurement of emission lines (especially broad-line and narrow-line Fe II emissions); the third criterion ensures the measurement of the AGN luminosity and the emission-line EWs suffering little from the contamination of the host-galaxy starlight. By combining SDSS spectra of high-luminosity QSOs and absorption-line or star-forming galaxies we find that our selection criteria corresponds to a galaxy contribution $\lesssim 10\%$ around 5100Å.

After removing duplications and sources with large number of bad pixels in the Hβ and Fe II λ4570 region, our final sample consists of 4178 type-1 AGNs (hereafter the full type 1 sample). Of them, 2092 have redshift $z \gtrsim 0.45$ and median S/N $\gtrsim 10$ per pixel in the UV Fe II region (2200–3090Å), which are used to examine the behavior of UV Fe II and Mg II $\lambda\lambda 2796, 2803$ doublet lines (hereafter λ2800), and referred to as the UV subsample.

2.1.2. Spectral fitting and measurements

We use the measured parameters from the Valued-added ExtraGAlactic Catalog developed and maintained by Center for Astrophysics, University of Science and Technology of China (USTC–

VEGAC; X.B. Dong et al., in preparation, J.G. Wang et al., in preparation). Details of spectral analysis will be described in separate papers. We discuss briefly here the steps relevant to this paper: we correct the SDSS spectra for Galactic extinction, separate Fe II emission from the continuum, and fit the emission lines. The optical Fe II is modeled with two separate sets of templates in *analytical* forms, one for the broad-line system and the other for *narrow-line* system, constructed from the measurements of I ZW 1 by Véron-Cetty et al. (2004) [see Dong et al. 2008 for details]. The regions of UV broad Fe II is modeled with the tabulated semiempirical template generated by Tsuzuki et al. (2006) basically from the measurements of I ZW 1; in the wavelength region covered by Mg II emission, this template also employs the calculation with the CLOUDY photoionization code (Ferland et al. 1998). Mg II doublet lines each is fitted with a truncated 5-parameter Gauss-Hermite series (Wang et al. 2009; see also Salvainder et al. 2007). As its profile is sometimes rather complex, broad-line Hβ is fitted with as many Gaussians as statistically justified; we do not ascribe any particular physical significance to the individual Gaussian components (Dong et al. 2005). Every broad Fe II lines are assumed to have the same profile as broad Hβ while the redshift of broad-line Fe II is set to be a free parameter; the uncertainty of the Fe II line width has little effect on the measurement of the Fe II flux (Salvainder et al. 2007, Hu et al. 2008). All narrow emission lines are fitted with a single Gaussian except the [O III] $\lambda\lambda$4959,5007 doublet; each line of the [O III] doublet is modeled with two Gaussians, with one accounting for the line core and the other for a possible blue wing as seen in many objects. The redshift and width of narrow-line Fe II are set to be free parameters.

Here we must note that, to properly measure the parameters of Fe II emission, the separation of narrow-line Fe II from the broad-line one is very important; as far as we know, this point has been long neglected mainly because of the lack of a narrow-line Fe II template until Véron-Cetty et al. (2004). Narrow Fe II multiplets, both permitted and forbidden, have been observed in the AGN spectra, both in the UV (e.g., Vestergaard & Wilkes 2001, Wang et al. 2008) and in the optical (e.g., Véron-Cetty et al. 2004, Véron-Cetty et al. 2007, Bruhweiler & Verner 2008; see also §4.6 of Hu et al. 2008). Certainly, whether there is a physically distinct boundary between the NLR and BLR of AGNs is still hotly debated (cf. Laor 2007), particularly considering the likely presence of the region intermediate between them (e.g., the Intermediate-Line Region [ILR], Brotherton et al. 1994; the inner NLR, Nagao et al. 2003, see Zhang et al. 2009 for a concise review); and both the BLR and NLR may be highly stratified and multi-zoned. In this paper, we follow Véron-Cetty et al. (2004) who phenomenologically took the Fe II component presented in other broad lines as the broad-line (L1), the Fe II (both permitted and forbidden) component presented in other low-excitation narrow lines the narrow-line (N3). In I ZW 1, there are two additional systems, N1 and N2, that appears only in high-excitation lines (not in Fe II); N1 and N2 are relatively broad and blueshifted by 1450 and 500 km s^{-1} respectively whereas N3 is almost at the systemic redshift of the host galaxy. The broad-line Fe II system of I ZW 1 is also blueshifted by about 150 – 200

km s^{-1} in both the optical and UV bands (Véron-Cetty et al. 2004, Laor et al. 1997; and Cf. Hu et al. 2008), which distinguishes it from the narrow-line system. The in-depth investigation on the physics of the narrow-line Fe II is beyond the scope of this paper and deferred to a forthcoming paper.

In Figure 1, we show the optical spectrum of a representative object in the present sample (SDSS J092801.30+491817.3), as well as the result of our spectral decomposition. In this object, the optical Fe II broad lines have a width of 1300 km s^{-1} FWHM; narrow Fe II, 250 km s^{-1} (corrected for the instrumental broadening of 130 km s^{-1} FWHM). Note that the individual narrow Fe II lines marked in the figure (particularly the forbidden lines) are separate from any broad Fe II lines, which indicates that our decomposed narrow Fe II multiplets are *bona fide*, not residuals from broad Fe II subtraction due to mismatch of the broad-line Fe II model. The AGNs with strong narrow-line Fe II emission are of diverse types: NLS1s and non-NLS1s, broad absorption-line (BAL) QSOs and non-BAL QSOs, radio-loud and radio-quiet. Figure 2 displays several diverse SDSS spectra with strong narrow Fe II emission in the sample, as well as our decomposition in the rest-wavelength range of 4000–5600Å; in its bottom panel, a low-ionization BAL QSO with variable, high radio luminosity (FBQS J152350.4+391405, $L_{5\mathrm{GHz}} = 4.0 \times 10^{31}$ ergs s^{-1} Hz^{-1}; Becker et al. 2000) is displayed. In Figure 3, we show the spectral fitting in the UV Fe II region.

For all measured emission-line fluxes, we regard the value as reliable when it is $\geq 2\sigma$; otherwise, we adopt the value plus the 2σ error as an upper limit. We calculate the black hole masses based on Hβ line using the relation presented in Vestergaard & Peterson (2006, their Eqn. 5). This relation was calibrated with reverberation mapping-based masses and used the R–L relation by Bentz et al. (2006) which was corrected for host-galaxy starlight contamination. The Eddington ratios are calculated assuming a bolometric luminosity correction $L_{\mathrm{bol}} \approx 9\lambda L_{\lambda}(5100)$ (Kaspi et al. 2000, Elvis et al. 1994). The mean and standard deviation (computed in log-space) of the FWHM of broad Hβ is 3600 km s^{-1} and 0.22 dex; $\lambda L_{\lambda}(5100)$, 4×10^{44}ergs s^{-1} and 0.40 dex; M_{BH}, $2 \times 10^{8} M_{\odot}$ and 0.52 dex; L/L_{Edd}, 0.13 and 0.44 dex. Because the SDSS spectroscopical survey is magnitude-limited, M_{BH} and L/L_{Edd} correlate with each other apparently; this apparent correlation is enhanced by the mutual dependence of both variables, by construction, on FWHM of broad Hβ and $\lambda L_{\lambda}(5100)$. The Spearman correlation coefficients (r_{s}) between M_{BH} and L/L_{Edd} are –0.663 for the full type 1 sample (4178 objects), and –0.762 for the UV subsample (2092 objects).

2.2. Correlation and regression

We use the generalized Spearman rank method implemented in the ASURV package (Isobe et al. 1986) to perform bivariate correlation test, and the generalized partial Spearman rank method to perform partial correlation test (Kendall & Stuart 1979; see, e.g., Shapley et al. 2001 for a previous

application). Both methods test for not only a linear relation but a monotonic one; and they can handle censored data in both independent and dependent variables. The results are summarized in Table 1, where we report the Spearman coefficient (r_s) and the probability (P_{null}) that a correlation is not present. Out of the correlation results, two striking features emerge as follows:

- According to the Spearman correlation analysis, the strongest correlations of almost all the emission-line intensity ratios and EWs are with L/L_{Edd}, rather than with L or M_{BH} itself.[3] This is confirmed by the Spearman partial correlation analysis: when controlling for linewidth, L or M_{BH}, there are still strong correlations with L/L_{Edd}, but *NOT vice versa*. Besides, generally line ratios have tighter correlations with L/L_{Edd} than the EWs of the related emission lines.

- The intensity ratios of Fe II emissions – both narrow and broad, both in the UV and in the optical – to Mg II λ2800 have very strong, positive correlations with L/L_{Edd}. Interestingly, (narrow Fe II)/Mg II has a stronger correlation with L/L_{Edd} than (broad Fe II)/Mg II (r_s= 0.74 versus 0.58 and 0.46).

In Figure 4, we plot the equivalent widths of the ultraviolet (2200 – 3090Å), optical (4434 – 4684Å) broad-line and narrow-line Fe II emissions versus λL_λ(5100Å), black hole mass, and Eddington ratio ($\ell \equiv L_{bol}/L_{Edd}$). In Figure 5, the three correlations of Fe II/Mg II ratios with L/L_{Edd} are illustrated; these tight correlations are striking considering the narrow range of L/L_{Edd} in our sample (1σ = 0.44 for a log-normal distribution) and the known systematical errors in the L/L_{Edd} estimation (see §3.1.1). We performed linear regressions in the log–log scale using the method of Kelly (2007). This method adopts a Bayesian approach and accounts for measurement errors, censoring and intrinsic scatter. The results are as follows,

$$\log \frac{\mathrm{FeII^N}\,\lambda 4570}{\mathrm{MgII}} = (-0.18 \pm 0.05) + (1.77 \pm 0.05)\log \ell \quad (1)$$

$$\log \frac{\mathrm{FeII^B}\,\lambda 4570}{\mathrm{MgII}} = (0.34 \pm 0.02) + (0.74 \pm 0.03)\log \ell \quad (2)$$

$$\log \frac{\mathrm{FeII\ UV}}{\mathrm{MgII}} = (0.94 \pm 0.01) + (0.33 \pm 0.02)\log \ell \quad (3)$$

[3]The only exception is the EW of broad Hβ. This is because a significant fraction of broad Hβ is emitted from the surface of the AD (and/or high-ionization, optically-thin clouds). We will discuss this point and other properties of broad Hβ in a forthcoming paper (see also §3.3). Note that Hydrogen Balmer lines, which can be produced through both the recombination process of H^+ ion and the collisional-excitation of H^0 atom, originates efficiently from both the fully ionized H^+ region and the partially ionized H I* region; thus the total emission of Balmer lines is hybrid, as suggested by mounting observational facts (see Marziani et al. 2008 and references therein; §4.2 of Wang et al. [2009]).

The intrinsic standard deviation of these relations (corrected for measurement errors) are 0.04, 0.22 and 0.15, respectively.

3. Results and Discussions

3.1. $L/L_{\rm Edd}$ controls Fe II strength

3.1.1. The phenomenological regularities

As shown above, a general trend is that the emission-line EWs and intensity ratios correlate more tightly with $L/L_{\rm Edd}$ than with L or $M_{\rm BH}$. In this paper we focus on the behaviors of the narrow-line and broad-line Fe II emissions, and defer the comprehensive discussions to an accompanying paper (Dong et al., 2009b). First, it is quite unexpected that narrow-line Fe II has a tighter correlation with $L/L_{\rm Edd}$ than broad-line Fe II, as the gas emitting broad-line Fe II is thought to be closer to and thus should be linked more tightly to the central engine than the narrow-line. One possible explanation is that the origin of narrow-line Fe II is more homogeneous than the broad-line (see §3.2 and 3.3). Second, the line ratios have stronger correlations with $L/L_{\rm Edd}$ than the EWs of narrow and broad Fe II. This is natural since, compared to line ratio, EW depends on more additional parameters such as the covering factor of the BLR and the anisotropy of the continuum radiation. The exceptions (see Table 1) are the correlations between line ratios and $L/L_{\rm Edd}$ that have a flat log–log slope, such as (narrow Fe II)/(broad Fe II); the dynamical range of the line ratio is small and the relation is dominated by fluctuation caused by the measurement errors. Third, UV Fe II has not as tight a correlation with $L/L_{\rm Edd}$ as the optical Fe II. This is caused by certain radiation transfer effects that we will discussed in Dong et al. (2009b). Fourth and probably the most important, as we mentioned in §2.2, in any case the ratios of Fe II to Mg II have quite tight correlations with $L/L_{\rm Edd}$, and yet not with L or $M_{\rm BH}$.

Collin et al. (2006) argued that the use of FWHM would introduce systematic biases to the virial $M_{\rm BH}$ estimate due to viewing angle effect and the presence of non-virialized velocity component(s) (see also Sulentic et al. 2006; Wang et al. 2009). We thus calculate $M_{\rm BH}$ also using the relation proposed by Collin et al. (2006, their Eqn. 7) and others; this alternative $M_{\rm BH}$ estimate leads to similar results. We note that, in the plot of (narrow Fe II)/Mg II versus $L/L_{\rm Edd}$ (panel c of Figure 4), there are some data points at the low $L/L_{\rm Edd}$ end (< 0.05) with systematically larger line ratios. This is likely caused by the over-estimated $M_{\rm BH}$ due to the systematic biases as suggested by those authors, which is confirmed by the correlation of the offset with FWHM ($r_{\rm s} = 0.46$ for the 1492 objects with reliably detected narrow Fe II). All the outliers with offsets of $\gtrsim 1$ dex upward have FWHM $\gtrsim 5500$ km s^{-1} (with the mean and standard deviation of 9200 and 2200 km s^{-1}). For such large FWHMs, even Collin et al.'s correction might be inadequate (in fact, Collin et

al.'s correction is by a factor of only 0.5 compared to the estimates of the Vestergaard & Peterson formalism). We will address this issue using a well-calibrated $M_{\rm BH}$ formalism with Mg II FWHM in Wang et al. (2009).

3.1.2. The physical picture

A strong, negative correlation between EW and $L/L_{\rm Edd}$ has been noted by several authors for C IV λ1549 line (Baskin & Laor 2004; see also Bachev et al. 2004). Both groups suggested that $L/L_{\rm Edd}$ is the fundamental driver of the Baldwin effect (BEff) – a well-known anticorrelation between the emission-line EWs and the AGN luminosity (Baldwin 1977), although they then did not know the underlying physical mechanism. The findings in this paper expand this picture. Although the gas environment in the line-emitting region of AGNs is complex and chaotic, the strength of almost all emission lines are governed by $L/L_{\rm Edd}$. It is well-known that C IV is a high-ionization line; Mg II, low-ionization and optically thick; and Fe II, low-ionization and optically thin (e.g., Collin-Souffrin et al. 1986). The emerging pattern is that, as $L/L_{\rm Edd}$ increases, the emission strength of high-ionization *or* optically thick lines decreases whereas the strength of low-ionization *and* optically thin lines increases.

High-ionization lines are emitted from the illuminated surface of the clouds; Optically thick lines, either from the illuminated surface (e.g. recombination line Lyα) or from the thin transition layer located immediately behind the Hydrogen ionization front (e.g., with the optical depth at the Lyman limit being in the range of 10 and 10^4 for low-ionization Mg II; Collin-Souffrin et al. 1986); yet low-ionization, optically thin lines such as Fe II multiplets arise from the partially ionized H I* region (i.e., from the ionization-bounded clouds only). Hence, the correlation pattern may be telling us that, as $L/L_{\rm Edd}$ increases, the column density ($N_{\rm H}$) of the clouds in the line-emitting region increases. We argue that the underlying physics is certain self-regulation mechanisms caused by (or corresponding to) Eddington ratio (dimensionless luminosity, not dimensionless accretion rate).[4] These mechanisms maintain the normal dynamically quasi-steady (or even quasi-virialized) states of the gas surrounding the central engine of AGNs; i.e., they regulate the global distributions of the properties of the clouds gravitationally bound in the line-emitting region (including the inner NLR, see §3.2). The details are beyond the scope of this paper, and are deferred to Dong et al. (2009b).

[4] Certainly, for particular radiation systems that are powered by gravitational accretion (e.g. AGNs), ℓ is linked tightly to $\dot{m}$ anyway (cf. Footnote 1; Merloni & Heinz 2008). Thus there is an additional effect associated with ℓ yet directly via $\dot{m}$ as follows. The increase in ℓ means, meanwhile, the increase in $\dot{m}$, the gas supply. Reasonably, it is from the supplied gas spiraling into the central engine that (at least a significant part of) the line-emitting clouds originate; this is particularly true for the BLR and inner NLR clouds that are located between the torus (as the fuel reservoir) and the accretion disk (e.g. Gaskell & Goosman 2008). Hence, as ℓ increases, the total mass of line-emitting gas increases.

Essentially, *there is a lower limit on the column density of clouds bound to the AGN line-emitting region, which is set by* $L/L_{\rm Edd}$. Even at $L/L_{\rm Edd} < 1$, low-$N_{\rm H}$ clouds are blown away because they are not massive enough to balance the radiation pressure force that is boosted by photoelectric absorption (see, e.g., Fabian et al. 2006, Marconi et al. 2008). According to Figure 1 of Fabian et al. (2006), for dust-free clouds of $N_{\rm H} \gtrsim 10^{21}$ cm^{-2}, the low limit is approximately proportional to $L/L_{\rm Edd}$ as $N_{\rm H} > 10^{23}\,\ell$ cm^{-2}; for dusty clouds, $N_{\rm H} > 5 \times 10^{23}\,\ell$ cm^{-2}.

Last, we note that the tight, positive Fe II/Mg II – $L/L_{\rm Edd}$ correlations cannot be caused (or enhanced) by any intrinsic relation between the Fe/Mg abundance ratio and $L/L_{\rm Edd}$ due to the possible starburst–AGN connection. Because in any plausible scenario of the connection that the AGN activity is triggered by the starburst (e.g. Sanders et al. 1988, Davies et al. 2007), no matter how long is the delay between the two events, the AGN is first fully accreting and then gradually weakening; this would imply that Fe/Mg abundance ratio would correlates *negatively* with $L/L_{\rm Edd}$ opposite to the trend we see here.

3.2. The site of the narrow-line Fe II emission

As discussed above, the tight correlation between narrow-line Fe II and $L/L_{\rm Edd}$ hints that the gas emitting narrow-line Fe II probably is very homogeneous and thus the emission is not affected significantly by additional parameters. To investigate this, we search the Fe II emission in all the $\sim 27,000$ type 2 AGNs in the SDSS DR4, which are selected according to the selection criteria of Kauffmann et al. (2003) and have S/N > 5 for Hβ, [O III] λ5007, Hα and [N II] λ6583 lines. The mean and standard deviation of their redshifts are 0.10 and 0.05 respectively. No Fe II emission is detected at $\geq 3\sigma$ significance *in any object in the sample*. Thus, according to the well-established unification scheme for Seyfert galaxies (e.g. Antonucci 1993), we conclude that *narrow-line Fe II originates purely from the gas bound in the inner NLR that locates closer to the central engine than the torus*. The inner edge of the dusty torus is known to be on scales of parsecs, roughly the dust sublimation radius; its extent is likely on scales of several tens of parsecs (e.g., Schmitt et al. 2003, Jaffe et al. 2004, Zhang et al. 2008).

3.3. The sites of the broad-line Fe II emission

In contrast to the narrow-line Fe II, the EWs of the broad-line Fe II emissions show at most a moderate correlation with $L/L_{\rm Edd}$. What caused the different behavior? A natural explanation is that broad Fe II does not originate from a unique site, i.e., not only from the clouds bound in the BLR. An additional site is plausibly the surface of the AD, which has been speculated and

argued for a long time (e.g. Collin-Souffrin et al. 1980, Murray & Chiang 1997, Zhang et al. 2006). The AD surface at radii of typically hundreds of $r_{\rm G}$ ($r_{\rm G} \equiv GM/c^2$) is argued to be an ideal site to emit low-ionization lines such as Balmer lines, Mg II λ2800 and the UV and optical Fe II (e.g. Collin-Souffrin 1987 et seq.). This is convincingly supported by the observations of low-ionization lines of double-peaked profile in a minority of AGNs (Balmer lines: e.g. Chen et al. 1989, Eracleous & Halpern 2003, Strateva et al. 2003; Mg II: e.g. Halpern et al. 1996), particularly by the discoveries of Balmer lines having, in addition to a symmetric broad component located at the system redshift, an separate, extremely broad double-peaked component that is apparently gravitationally redshifted (Chen et al. 1989, Wang et al. 2005; see a treatment for the general case of twisted, warped disk in Wu et al. 2008). This disk component constitutes partly the often-called "red shelf" or "very broad component" (see, e.g., Sulentic et al. 2000) of the Balmer-line profile. In fact, double-peaked Fe II emission lines are observed in some disk-accreting systems such as cataclysmic variable stars, together with other double-peaked low-ionization lines such as Balmer lines, Ca II, Si II and He I lines that arise definitely from the AD according to Doppler tomography (e.g. Roelofs et al. 2006, Smith et al. 2006).

Note that the AD radii that can emit low-ionization lines are less than the critical radius of the gravitationally unstable part of the AD, $r_{\rm crit} \approx 2\times10^4\,(M_{\rm BH}/10^7 M_\odot)^{-0.46}\,r_{\rm G}$ (Collin & Huré 2001). It is argued that *the gravitationally unstable disk is one source of the clouds bound in the line-emitting region of AGNs, particularly for low-ionization lines such as Mg II and both narrow and broad Fe II as suggested in this paper* (Collin & Huré 2001; see also Leighly 2004); other sources of the clouds can be outflows that are liable to fragmentation (Proga et al. 2008) and gas infalling from the torus (Gaskell & Goosmann 2008). Compared to the gas in the torus, these clouds have less or even no dust.

Finally, we must mention that, in such high-density and high-column density clouds, some researchers have argued that photoionization heating might not be sufficient, additional heating like a mechanical one seems be necessary to strengthen the H I* region (e.g., Véron-Cetty et al. 2006, Joly et al. 2008). There is evidence that mechanical heating from outflows may be such a source (S.-H. Zhang, in preparation), although its contribution is generally expected not to be very significant and hard to estimate observationally. Outflows, which are launched from the AD — dependent on $L/L_{\rm Edd}$ in a certain way, can have large inclination angles or even equatorial (Murray et al. 1995, Proga et al. 2008), and thus collide with clouds in the line-emitting region or even in the torus. The collisions would also increase clouds in the BLR and inner NLR.

4. Conclusions and implications

In this paper, we find that the narrow-line Fe II originates purely from the inner NLR on scales less than the torus. Yet, the sites of the broad-line Fe II are likely to be not unique: similar to the situation of broad Hβ (probably to a less degree), a significant fraction of the emission is from the surface of the accretion disk instead of the clouds bound in the BLR. In summary, Fe II emission will arise from any gas surrounding the central engine of AGNs that has sufficiently high density, column density and heating energy input, and at the same time has very low dust content.

More importantly, although the excitation mechanisms of Fe II emission (and the sites for the broad-line one) are complex, its relative strengths with respect to both the continuum and other emission lines (particularly Mg II) correlate tightly and positively with $L/L_{\rm Edd}$, and intrinsically *not* with AGN luminosity or $M_{\rm BH}$. That is, in addition to the global similarity (to the 0th-order approximation) of the QSO spectra, the 1st-order variation of the emission lines are controlled by $L/L_{\rm Edd}$. The essential underlying physical mechanism of these correlations is that Eddington ratio (dimensionless luminosity, $\ell \equiv L/L_{\rm Edd}$, see Footnote 1) regulates the distribution of the column density of the clouds bound in the line-emitting region. We will discuss it further in an accompanying paper, including its implication to the BEff and its second-order effects (Dong et al. 2009b). One possible interesting implication is that, as far as spectral correlations in the UV–optical band are concerned (particularly the Fe II – [O III] anticorrelation), BG92's PC1 could share the same origin – $L/L_{\rm Edd}$ – with PC2, which is exactly the BEff of He II λ4686 line (BG92, Wills et al. 1999; see Dietrich et al. 2002 for an investigation of the He II BEff).

If the observed large scatter of Fe II/Mg II at the same redshift is caused predominately by the diversity of $L/L_{\rm Edd}$, then it is hopeful to still use Fe II/Mg II as a measure of the Fe/Mg abundance ratio to study the chemical evolutionary history of the gas surrounding AGNs and to constrain its age ("cosmic clock"), once the systematic variation caused by $L/L_{\rm Edd}$ is corrected according to the formalisms (Eqn. 1–3) presented in this paper. We will address this issue in a forthcoming paper (H.Y. Wang et al., in preparation).

DXB thanks Kirk Korista, Martin Gaskell, Aaron Barth, Alessandro Marconi, Philippe Véron, Daniel Proga and Xueguang Zhang for the helpful discussions and comments, thanks Monique Joly and Feng Yuan for useful comments, and thanks Sheng-Miao Wu, Lei Chen and Fu-Guo Xie for their warm hospitality and brainstorming discussions during my two visits in Shanghai Observatory. We thank Zhen-Ya Zheng for the help in improving IDL figures. This work is supported by Chinese NSF grants NSF-10533050, NSF-10703006 and NSF-10728307, a CAS Knowledge Innovation Program (Grant No. KJCX2-YW-T05), and a National 973 Project of China (2007CB815403). Funding for the SDSS and SDSS-II has been provided by the Alfred P. Sloan Foundation, the Participating Institutions, the National Science Foundation, the U.S. Department

of Energy, the National Aeronautics and Space Administration, the Japanese Monbukagakusho, the Max Planck Society, and the Higher Education Funding Council for England. The SDSS Web Site is http://www.sdss.org/. The SDSS is managed by the Astrophysical Research Consortium for the Participating Institutions. The Participating Institutions are the American Museum of Natural History, Astrophysical Institute Potsdam, University of Basel, University of Cambridge, Case Western Reserve University, University of Chicago, Drexel University, Fermilab, the Institute for Advanced Study, the Japan Participation Group, Johns Hopkins University, the Joint Institute for Nuclear Astrophysics, the Kavli Institute for Particle Astrophysics and Cosmology, the Korean Scientist Group, the Chinese Academy of Sciences (LAMOST), Los Alamos National Laboratory, the Max-Planck-Institute for Astronomy (MPIA), the Max-Planck-Institute for Astrophysics (MPA), New Mexico State University, Ohio State University, University of Pittsburgh, University of Portsmouth, Princeton University, the United States Naval Observatory, and the University of Washington.

REFERENCES

Adelman-McCarthy, J. K., et al. 2006, ApJS, 162, 38

Antonucci, R. 1993, ARA&A,31, 473

Bachev, R., Marziani, P., Sulentic, J. W., Zamanov, R., Calvani, M., & Dultzin-Hacyan, D. 2004, ApJ, 617, 171

Baldwin, J. A. 1977, ApJ, 214, 679

Baldwin, J., Ferland, G., Korista, K., & Verner, D. 1995, ApJ, 455, L119

Baldwin, J. A., Ferland, G. J., Korista, K. T., Hamann, F., & LaCluyzé, A. 2004, ApJ, 615, 610

Baskin, A., & Laor, A. 2004, MNRAS, 350, L31

Becker, R. H., White, R. L., Gregg, M. D., Brotherton, M. S., Laurent-Muehleisen, S. A., & Arav, N. 2000, ApJ, 538, 72

Bentz, M. C., Peterson, B. M., Pogge, R. W., Vestergaard, M., & Onken, C. A. 2006, ApJ, 644, 133

Boroson, T. A. & Green, R. F. 1992, ApJS, 80, 109 (BG92)

Boroson, T. A. 2002, ApJ, 565, 78

Brotherton, M. S., Wills, B. J., Francis, P. J., & Steidel, C. C. 1994, ApJ, 430, 495

Bruhweiler, F., & Verner, E. 2008, ApJ, 675, 83

Chen, K., Halpern, J. P., & Filippenko, A. V. 1989, ApJ, 339, 742

Collin-Souffrin, S., Joly, M., Dumont, S., & Heidmann, N. 1980, A&A, 83, 190

Collin-Souffrin, S., Joly, M., Pequignot, D., & Dumont, S. 1986, A&A, 166, 27

Collin-Souffrin, S. 1987, A&A, 179, 60

Collin, S., & Joly, M. 2000, New Astronomy Review, 44, 531

Collin, S., & Huré, J.-M. 2001, A&A, 372, 50

Davidson, K., & Netzer, H. 1979, Reviews of Modern Physics, 51, 715

Davies, R. I., Mueller Sánchez, F., Genzel, R., Tacconi, L. J., Hicks, E. K. S., Friedrich, S., & Sternberg, A. 2007, ApJ, 671, 1388

Dietrich, M., Hamann, F., Shields, J. C., Constantin, A., Vestergaard, M., Chaffee, F., Foltz, C. B., & Junkkarinen, V. T. 2002, ApJ, 581, 912

Dong, X.-B., Zhou, H.-Y., Wang, T.-G., Wang, J.-X., Li, C., & Zhou, Y.-Y. 2005, ApJ, 620, 629

Dong, X., Wang, T., Wang, J., Yuan, W., Zhou, H., Dai, H., & Zhang, K. 2008, MNRAS, 383, 581

Dong, X.-B., Wang, T.-G., Wang, J.-G., Wang, H.-Y., Fan, X.-H., Zhou, H.-Y., Yuan, W.-M., Long, Q. 2009b, submitted to ApJ

Elston, R., Thompson, K. L., & Hill, G. J. 1994, Nature, 367, 250

Elvis, M., et al. 1994, ApJS, 95, 1

Fabian, A. C., Celotti, A., & Erlund, M. C. 2006, MNRAS, 373, L16

Ferland, G. J., Korista, K. T., Verner, D. A., Ferguson, J. W., Kingdon, J. B., & Verner, E. M. 1998, PASP, 110, 761

Freudling, W., Corbin, M. R., & Korista, K. T. 2003, ApJ, 587, L67

Gaskell, C. M., Goosmann, R. W., Antonucci, R. R. J., & Whysong, D. H. 2004, ApJ, 616, 147

Gaskell, C. M., Klimek, E. S., & Nazarova, L. S. 2007, arXiv:0711.1025

Gaskell, C. M., & Benker, A. J. 2007, arXiv:0711.1013

Gaskell, C. M., & Goosmann, R. W. 2008, arXiv:0805.4258

Halpern, J. P., Eracleous, M., Filippenko, A. V., & Chen, K. 1996, ApJ, 464, 704

Hamann, F., & Ferland, G. 1993, ApJ, 418, 11

Hu, C., Wang, J.-M., Ho, L. C., Chen, Y.-M., Zhang, H.-T., Bian, W.-H., & Xue, S.-J. 2008, ApJ, 687, 78

Isobe, T., Feigelson, E. D., & Nelson, P. I. 1986, ApJ, 306, 490

Iwamuro, F., Kimura, M., Eto, S., Maihara, T., Motohara, K., Yoshii, Y., & Doi, M. 2004, ApJ, 614, 69

Jaffe, W., et al. 2004, Nature, 429, 47

Jiang, L., Fan, X., Vestergaard, M., Kurk, J. D., Walter, F., Kelly, B. C., & Strauss, M. A. 2007, AJ, 134, 1150

Joly, M., Véron-Cetty, M., & Véron, P. 2008, Revista Mexicana de Astronomia y Astrofisica Conference Series, 32, 59

Kaspi, S., Smith, P. S., Netzer, H., Maoz, D., Jannuzi, B. T., & Giveon, U., 2000, ApJ, 533, 631

Kauffmann, G., et al. 2003, MNRAS, 346, 1055

Kelly, B. C. 2007, ApJ, 665, 1489

Kendall, M., & Stuart, A. 1979, The advanced theory of statistics. Vol.2: Inference and relationship, London: Griffin, 1979, 4th ed.

Kollatschny, W., & Welsh, W. F. 2001, in ASP Conf. Ser. 224, Probing the Physics of Active Galactic Nuclei, 449

Korista, K. 1999, in ASP Conf. Ser. 162, Quasars and Cosmology, 429

Korista, K. T., & Goad, M. R. 2000, ApJ, 536, 284

Kuehn, C. A., Baldwin, J. A., Peterson, B. M., & Korista, K. T. 2008, ApJ, 673, 69

Kurk, J. D., et al. 2007, ApJ, 669, 32

Laor, A., Jannuzi, B. T., Green, R. F., & Boroson, T. A. 1997, ApJ, 489, 656

Laor, A. 2007, in ASP Conf. Ser. 373, The Central Engine of Active Galactic Nuclei, 384

Leighly, K. M. 2004, ApJ, 611, 125

Leighly, K. M., & Moore, J. R. 2006, ApJ, 644, 748

Maoz, D. 2007, MNRAS, 377, 1696

Marconi, A., Axon, D. J., Maiolino, R., Nagao, T., Pastorini, G., Pietrini, P., Robinson, A., & Torricelli, G. 2008, ApJ, 678, 693

Marziani, P., Sulentic, J. W., & Dultzin, D. 2008, Revista Mexicana de Astronomia y Astrofisica Conference Series, 32, 69

Matsuoka, Y., Oyabu, S., Tsuzuki, Y., & Kawara, K. 2007, ApJ, 663, 781

Matteucci, F., & Recchi, S. 2001, ApJ, 558, 351

Merloni, A., & Heinz, S. 2008, MNRAS, 388, 1011

Moran, E. C., Filippenko, A. V., Ho, L. C., Shields, J. C., Belloni, T., Comastri, A., Snowden, S. L., & Sramek, R. A. 1999, PASP, 111, 801

Murray, N., Chiang, J., Grossman, S. A., & Voit, G. M. 1995, ApJ, 451, 498

Murray, N., & Chiang, J. 1997, ApJ, 474, 91

Nagao, T., Murayama, T., Shioya, Y., & Taniguchi, Y. 2003, AJ, 126, 1167

Proga, D., Ostriker, J. P., & Kurosawa, R. 2008, ApJ, 676, 101

Roelofs, G. H. A., Groot, P. J., Marsh, T. R., Steeghs, D., & Nelemans, G. 2006, MNRAS, 365, 1109

Salviander, S., et al., 2007, ApJ, 662, 131

Sanders, D. B., Soifer, B. T., Elias, J. H., Madore, B. F., Matthews, K., Neugebauer, G., & Scoville, N. Z. 1988, ApJ, 325, 74

Schlegel, D. J., Finkbeiner, D. P., & Davis, M. 1998, ApJ, 500, 525

Schmitt, H. R.; Donley, J. L.; Antonucci, R. R. J.; Hutchings, J. B.; Kinney, A. L.; Pringle, J. E., 2003, ApJ, 597, 768

Shakura, N. I., & Syunyaev, R. A. 1973, A&A, 24, 337

Shapley, A., Fabbiano, G., & Eskridge, P. B. 2001, ApJS, 137, 139

Smith, A. J., Haswell, C. A., & Hynes, R. I. 2006, MNRAS, 369, 1537

Sulentic, J. W., Zwitter, T., Marziani, P., & Dultzin-Hacyan, D. 2000, ApJ, 536, L5

Sulentic, J. W., Marziani, P., & Dultzin-Hacyan, D. 2000, ARA&A, 38, 521

Sulentic, J. M. et al., 2006, A&A, 456, 929S

Tsuzuki, Y., Kawara, K., Yoshii, Y., Oyabu, S., Tanabé, T., & Matsuoka, Y. 2006, ApJ, 650, 57

Véron-Cetty, M.-P., Joly, M., & Véron, P. 2004, A&A, 417, 515

Véron-Cetty, M.-P., Joly, M., Véron, P., Boroson, T., Lipari, S., & Ogle, P. 2006, A&A, 451, 851

Véron-Cetty, M.-P., Véron, P., Joly, M., & Kollatschny, W. 2007, A&A, 475, 487

Vestergaard, M., & Wilkes, B. J. 2001, ApJS, 134, 1

Vestergaard, M., & Peterson, B. M. 2005, ApJ, 625, 688

Vestergaard, M., & Peterson, B. M. 2006, ApJ, 641, 689

Wang, J., Wei, J. Y., & He, X. T. 2005, A&A, 436, 417

Wang, J.-G., Dong, X.-B., Wang, T.-G., Yuan, W.-M., Zhang, K., Wang, H.-Y., Zhang, S.-H., and Zhou, H.-Y. 2009, submitted to ApJ

Wang, T.-G., Dong, X.-B., Zhang, X.-G., Zhou, H.-Y., Wang, J.-X., & Lu, Y.-J. 2005, ApJ, 625, L35

Wang, T., Dai, H., & Zhou, H. 2008, ApJ, 674, 668

Wills, B. J., Laor, A., Brotherton, M. S., Wills, D., Wilkes, B. J., Ferland, G. J., & Shang, Z. 1999, ApJ, 515, L53

Wu, S.-M., Wang, T.-G., & Dong, X.-B. 2008, MNRAS, 389, 213

York, D. G. et al. 2000, AJ, 120, 1579

Yoshii, Y., Tsujimoto, T., & Kawara, K. 1998, ApJ, 507, L113

Zhang, K., Wang, T., Dong, X., & Lu, H. 2008, ApJ, 685, L109

Zhang, K., Wang, T., Dong, X., Zhou, H., & Lu, H. 2009, arXiv:0902.4390

Zhang, X.-G., Dultzin-Hacyan, D., & Wang, T.-G. 2006, MNRAS, 372, L5

Zhang, X.-G., Dultzin-Hacyan, D., & Wang, T.-G. 2007, Revista Mexicana de Astronomia y Astrofisica, 43, 101

This preprint was prepared with the AAS LaTeX macros v5.2.

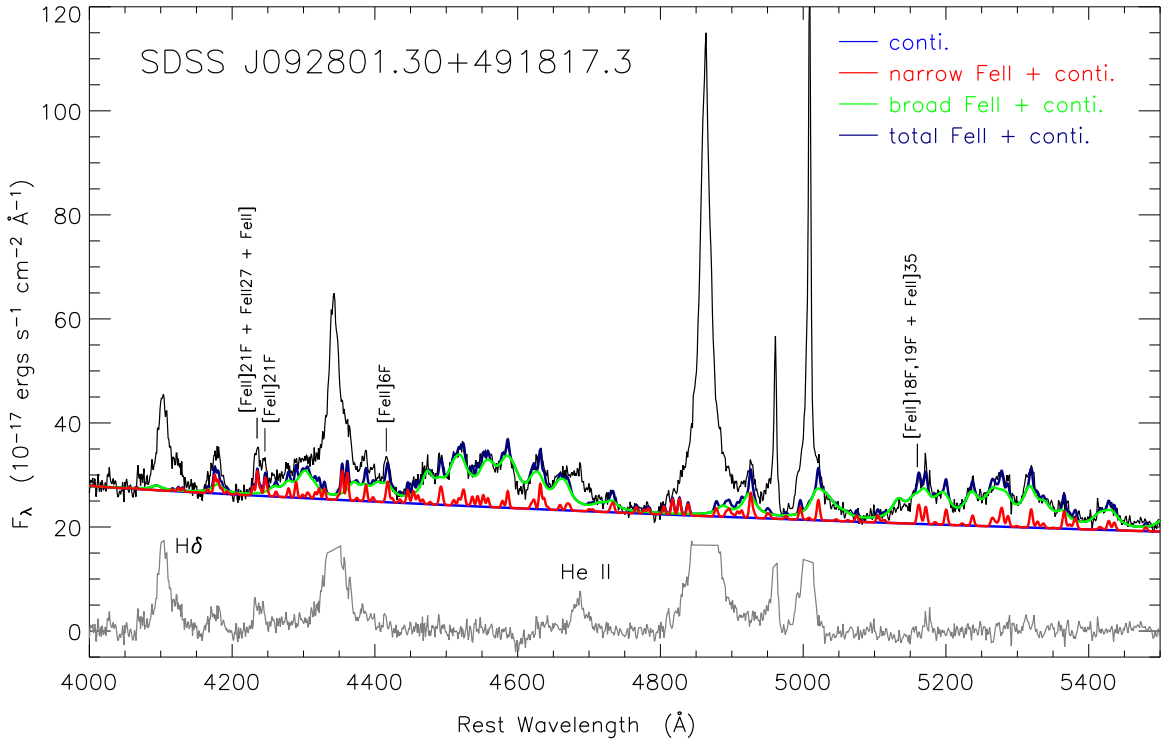

Fig. 1.— Demonstration of spectral fitting in the optical region. In the figure, we show: the SDSS spectrum (black), the local AGN continuum (blue), the continuum plus narrow-line Fe II complex emission (red), the continuum plus broad-line Fe II complex emission (green), the pseudocontinuum (continuum plus total Fe II, navy), and the pseudocontinuum subtracted residual (gray). Also marked are some narrow Fe II lines (particularly the forbidden lines) that are separate from any broad Fe II lines. The strong emission lines in the residual spectrum are chopped for clarity.

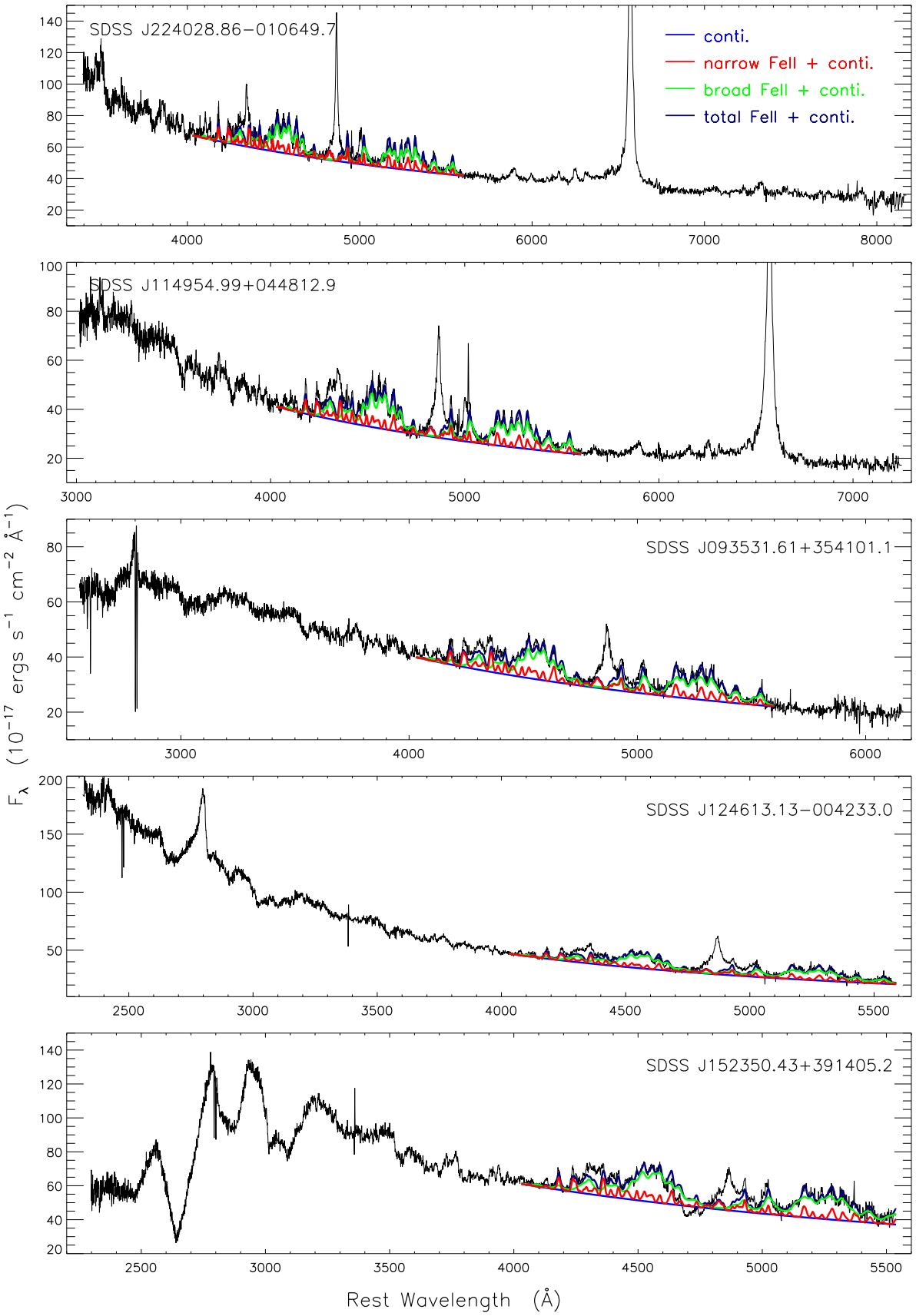

Fig. 2.— Demonstration of the SDSS spectra of several strong narrow Fe II emitting AGNs of

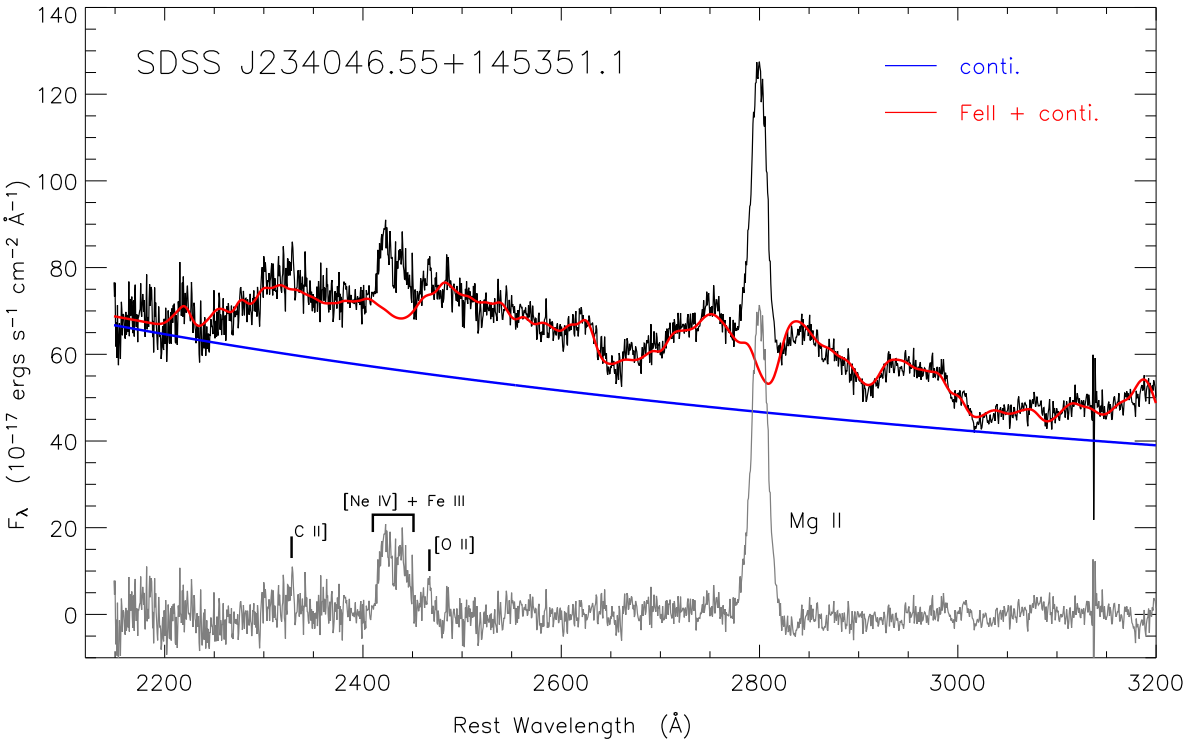

Fig. 3.— Demonstration of spectral fitting in the ultraviolet region. In the figure, we show: The SDSS spectrum (black), the local AGN continuum (blue), the pseudocontinuum (continuum plus Fe II complex emission, red), and the pseudocontinuum subtracted residual (gray).

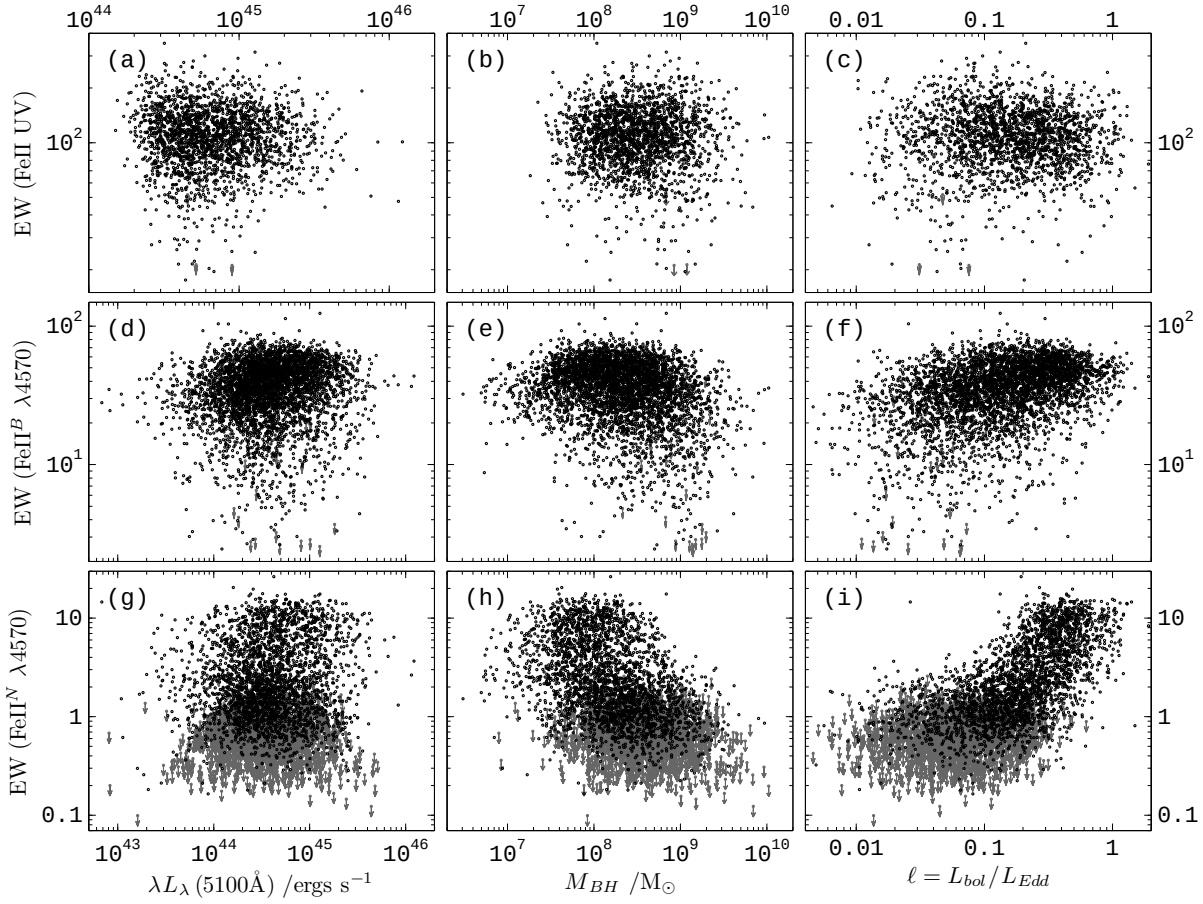

Fig. 4.— The relation between the equivalent widths of the ultraviolet (2200 – 3090Å), the optical (4434 – 4684Å) broad-line and narrow-line Fe II emissions of type-1 AGNs and their λL_λ(5100Å), black hole mass ($M_{\rm BH}$), and Eddington ratio ($\ell \equiv L_{\rm bol}/L_{\rm Edd}$).

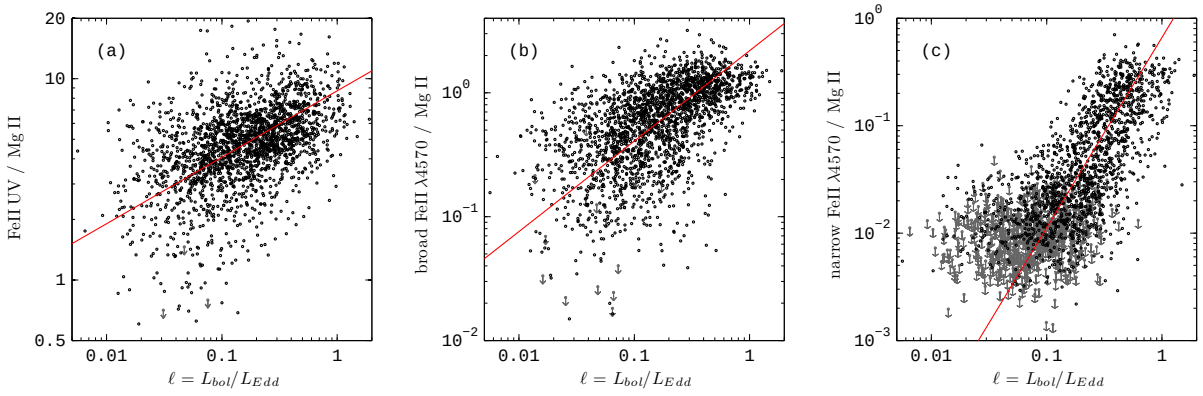

Fig. 5.— The relation between the intensity ratios and Eddington ratio for type-1 AGNs. Also plotted are the respective best-fitted linear relation in the log–log scale (see Eqn. 1–3). Note that in panel (c) there are some outliers at the low $L/L_{\rm Edd}$ end with systematically larger line ratios (e.g., by 1 dex); this is likely caused by the over-estimated $M_{\rm BH}$ due to some systematic biases because all the outliers have FWHM $\gtrsim$ 5500 km s^{-1} (with the mean and standard deviation being 9200 and 2200 km s^{-1}).

Table 1: Results of Spearman correlation and partial correlation analysis [a]

X	FWHM (H$\beta^{\rm B}$)	$\lambda L_\lambda(5100)$	$M_{\rm BH}$ [b]	$L/L_{\rm Edd}$ [b]	(X, $L/L_{\rm Edd}$; $M_{\rm BH}$) [c]	(X, $M_{\rm BH}$; $L/L_{\rm Edd}$) [c]
EW (FeII$^{\rm N}$ 4570)	–0.659 (<1e-14)	0.102 (<1e-14)	–0.508 (<1e-14)	0.708 (<1e-14)	0.576 (<1e-14)	–0.073 (2e-06)
(FeII^{N} 4570)/MgII	–0.731 (<1e-14)	0.097 (<1e-14)	–0.627 (<1e-14)	0.745 (<1e-14)	0.530 (<1e-14)	–0.137 (3e-10)
(FeII^{N} 4570)/H$\beta^{\rm B}$	–0.680 (<1e-14)	0.079 (<1e-14)	–0.537 (<1e-14)	0.720 (<1e-14)	0.576 (<1e-14)	–0.115 (9e-14)
(FeII^{N} 4570)/[O III] 5007	–0.606 (<1e-14)	0.140 (<1e-14)	–0.440 (<1e-14)	0.666 (<1e-14)	0.557 (<1e-14)	0.003 (9e-01)
EW (FeII$^{\rm B}$ 4570)	–0.333 (<1e-14)	0.156 (<1e-14)	–0.230 (<1e-14)	0.396 (<1e-14)	0.334 (<1e-14)	0.047 (2e-03)
(FeII^{B} 4570)/MgII	–0.567 (<1e-14)	0.116 (<1e-14)	–0.480 (<1e-14)	0.585 (<1e-14)	0.386 (<1e-14)	–0.065 (3e-03)
(FeII^{B} 4570)/H$\beta^{\rm B}$	–0.474 (<1e-14)	0.064 (<1e-14)	–0.373 (<1e-14)	0.499 (<1e-14)	0.362 (<1e-14)	–0.065 (3e-05)
(FeII^{B} 4570)/[O III] 5007	–0.244 (<1e-14)	0.174 (<1e-14)	–0.141 (<1e-14)	0.321 (<1e-14)	0.307 (<1e-14)	0.101 (5e-11)
EW (FeII UV)	0.023 (3e-01)	–0.036 (1e-01)	–0.001 (1e+00)	–0.041 (6e-02)	–0.064 (3e-03)	–0.050 (2e-02)
(FeII UV)/MgII	–0.429 (<1e-14)	0.157 (<1e-14)	–0.342 (<1e-14)	0.465 (<1e-14)	0.336 (<1e-14)	0.022 (3e-01)
(FeII UV)/H$\beta^{\rm B}$	–0.159 (<1e-14)	0.044 (4e-02)	–0.135 (<1e-14)	0.164 (<1e-14)	0.095 (1e-05)	–0.016 (5e-01)
(FeII UV)/[O III] 5007	–0.079 (3e-04)	0.103 (<1e-14)	–0.040 (7e-02)	0.107 (<1e-14)	0.118 (6e-08)	0.064 (3e-03)
(FeII^{N} 4570)/(FeII UV)	–0.698 (<1e-14)	0.060 (6e-03)	–0.604 (<1e-14)	0.701 (<1e-14)	0.466 (<1e-14)	–0.151 (3e-12)
(FeII^{B} 4570)/(FeII UV)	–0.435 (<1e-14)	0.042 (5e-02)	–0.383 (<1e-14)	0.435 (<1e-14)	0.239 (<1e-14)	–0.088 (5e-05)
(FeII^{N} 4570)/(FeII^{B} 4570)	–0.584 (<1e-14)	0.066 (2e-05)	–0.453 (<1e-14)	0.619 (<1e-14)	0.477 (<1e-14)	–0.072 (3e-06)
EW ([O III] 5007)	0.104 (<1e-14)	–0.098 (<1e-14)	0.045 (4e-03)	–0.152 (<1e-14)	–0.163 (<1e-14)	–0.075 (1e-06)
EW (H$\beta^{\rm B}$)	0.333 (<1e-14)	0.110 (<1e-14)	0.309 (<1e-14)	–0.288 (<1e-14)	–0.117 (4e-14)	0.165 (<1e-14)
EW (Mg II)	0.496 (<1e-14)	–0.216 (<1e-14)	0.378 (<1e-14)	–0.553 (<1e-14)	–0.442 (<1e-14)	–0.080 (2e-04)

[a] For each entry, we list the Spearman rank correlation coefficient ($r_{\rm s}$) and the probability of the null hypothesis ($P_{\rm null}$) in parenthesis.

[b] The black hole masses are calculated using the formalism presented in Vestergaard & Peterson (2006); Eddington ratios ($L/L_{\rm Edd}$) are calculated assuming that the bolometric luminosity $L_{\rm bol} \approx 9\lambda L_\lambda(5100)$.

[c] $(X, Y; Z)$ denotes the partial correlation between X and Y, controlling for Z.